doi:10.3772/j.issn.1006-6748.2021.04.008

Parametric sensitivity analysis of bearing characteristics of single DOF autonomous system of magnetic-liquid double suspension bearing①

Zhao Jianhua (赵建华)② * ** ***, Wang Qiang *, Wang Jin *, Wang Ziqi *, Zhang Bin *, Chen Tao *, Du Guojun * ** ***, Gao Dianrong * ** ***

(* Fluid Power Transmission and Control Laboratory, Yanshan University, Qinhuangdao 066004, P. R. China)

(** College of Civil Engineering and Mechanics, Yanshan University, Qinhuangdao 066004, P. R. China)

(*** Jiangsu Provincial Key Laboratory of Advanced Manufacture and Process for Marine Mechanical Equipment, Zhenjiang 212003, P. R. China)

Abstract

The mathematical model of single degree of freedom (DOF) nonlinear autonomous bearing system under constant flow supporting model is deduced. The single DOF nonlinear autonomous bearing system is transformed with the method of linear and nonlinear treatment, the mathematical expression and parameters sensitivity of relative error of stiffness and damping are presented. Finally, the main factors of magnetic-liquid double suspension bearing (MLDSB) are analyzed, and the influence on bearing performance indicators of single DOF nonlinear autonomous bearing system of main factors is revealed. The results show that linear stiffness/damping is the first part of equivalent stiffness/damping, and the second and third parts are high order minor term of Tayor series transform. The film thickness, the magnetic-liquid proportionality coefficient, the mass of rotor are the major influence factor of the bearing performance. The research can provide the theoretical reference for the design and nonlinear analysis of MLDSB.

Key words: magnetic-liquid double suspension bearing (MLDSB), nonlinear autonomous bearing system, equivalent nonlinear treatment, bearing performance indicator, parameter sensitivity, relative error

0 Introduction

Magnetic-liquid double suspension bearing (MLDSB) is mainly supported by electromagnetic suspension system and supplemented by hydrostatic bearing system, and then the phenomenons of poor load capacity, overload, seizing, bush-burning should be effectively avoided[1-5].

In recent years, many scholars have researched deeply on the nonlinear feature of hydrostatic bearing and electromagnetic suspension bearing, and have achieved fruitful research results. In Ref. [6], the nonlinear vibration of a single degree of freedom (DOF) rotor supported by active magnetic bearing (AMB) system was investigated. The typical nonlinear phenomena such as softening/hardening spring characteristic, jumps of the resonance curve can be observed and analyzed. In Ref. [7], the nonlinear dynamic behavior and stability of AMB-rotor system were studied by the Floquet theory. At the same time, the method consisting of a predictor-corrector mechanism and Netwon-Raphson method was presented to calculate critical speed corresponding to Hopf bifurcation point of the system. Ref. [8] showed that there were plenty of nonlinear phenomena such as periodic motion, almost periodic motion and chaotic motion in the process of system operation. Ref. [9] solved the nonlinear oil film force of the fixed-tilting tile sliding bearing by using the variational principle. And the influence of bearing fulcrum position and preload on the stability of the rotor was obtained by using point mapping and Runge-Kutta method analysis. Ref. [10] established the nonlinear axis of the trajectory mathematical model of four-oil cavity hydrostatic bearing. The influence of rotor speed, oil supply pressure and radius clearance of the bearing on the nonlinear axis locus is studied, and the change law of axis locus under dynamic load is calculated.

① Supported by the National Natural Science Foundation of China (No. 51705445), General Project of Natural Science Foundation of Hebei Province (No. E2016203324) and Youth Fund Project of Scientific Research Project of Hebei University (No. QN202013).

② To whom correspondence should be addressed. E-mail: zhaojianhua@ysu.edu.cn

Received on July 26, 2020

The electromagnetic suspension system and hydrostatic bearing system are inter-coupled, and the nonlinear degree of MLDSB is sharply increased. It is necessary to find a simple method which can be mastered by engineering designers and reflect the nonlinear features of MLDSB[11-12].

The equivalent linearization treatment is used to dispose single DOF bearing system of MLDSB. The mathematical expressions and sensitivity of parameters of equivalent stiffness/damping and the relative errors of stiffness/damping are obtained. Primary and secondary orders of bearing indicators of single DOF autonomous system are extracted, and the influencing rules of the major influence factors on the performance of MLDSB are revealed. Therefore, the research in the article can provide theoretical reference for the design and performance analysis of MLDSB.

1 Mathematical model

Eight magnetic poles are symmetrically distributed in the circumferential direction of MLDSB. And the adjacent opposite poles are a pair of magnetic poles. Initially, the electromagnetic force and hydrostatic force by each pair of magnetic poles are equal. A pair of magnetic poles are analyzed as a support unit. Single DOF bearing system in the vertical direction of MLDSB is taken as the research object. As shown in Fig. 1, the bearing system is composed of rotor, upper and lower supporting units.

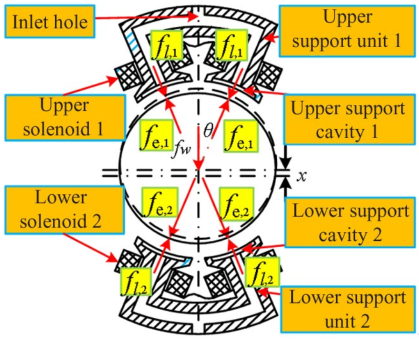

Fig. 1 Force diagram of single DOF of MLDSB

In order to research the bearing performance of MLDSB, the assumptions are as follows[13-14].

(1) The flow state of the lubricant is laminar flow, and the liquid inertial force is ignored.

(2) The viscosity of the liquid is ignored.

(3) Leakage magnetic flux is ignored.

(4) The magnetic resistance in the core and rotor is ignored, and the magnetic potential is only applied to the air gap.

(5) The influences of hysteresis and eddy current of magnetic materials are ignored.

(6) Gravity of bearing and rotor are ignored.

The initial design parameters of MLDSB are shown in Table 1.

Table 1 Design parameters of MLDSB

Mass of bearing m/kg	Elastic modulus E/MPa	Zinc coating thickness l/mm	Magnetic pole area A/mm^2
88.62×10^3	1.30×10^3	0.50	1000
Solenoid number N/Dimensionless	Cavity wedth A/m	Cavity length B/m	Axial sealing band width b/m
633	0.1	0.02	0.004
Circumferential sealing band width a/m	Pumping pressure p_s/MPa	Cavity pressure p/MPa	Bias current i_0/A
0.006	3.00	0.64	1.20
Film thickness h_0/μm	Sensitive oil-way volume V_{oa}/m^3	Air permeability μ_0/(H/m)	Magnetic-liquid proportionality coefficient K/Dimensionless
30	1.0×10^{-6}	$4\pi\times10^{-6}$	1.00

1.1 Initial state of single DOF bearing system

In the initial state, the rotor is located in the rotation center of the bearing. And film thickness of upper and lower bearing cavities is equal. The bias voltage of proportional valve and the bias current of electromagnet are equal respectively.

Flow of proportional valve The initial bias voltage of the proportional valve is set to u_0, and the output flow equation is as

$$q_{f,1,0} = q_{f,2,0} = k_1 u_0 \tag{1}$$

where, $q_{f,0}$ is output flow of proportional valve, L/min; k_1 is flow-voltage coefficient, L/min/V; u_0 is bias voltage of proportional valve, V.

Liquid resistance of bearing cavity Upper and lower bearing cavities of MLDSB can be simplified as rectangular structures. The liquid resistance equations are obtained as

$$R_{1,0} = R_{2,0} = \frac{\mu}{\bar{B}h_0^3} \tag{2}$$

where, R_0 is liquid resistance of bearing cavity, Pa · s/m^3; μ is dynamic viscosity of lubricant, Pa · s; $\bar{B}$ is bearing flow coefficient of bearing cavity, dimensionless; h_0 is film thickness of bearing cavity, m.

Hydrostatic bearing force According to Navier-Stokes equation[15], the hydrostatic bearing forces of upper and lower bearing cavities are obtained as

$$\begin{cases} f_{l,,1,0} = 2q_{1,0}R_{1,0}A_e\cos\theta \\ f_{l,,2,0} = 2q_{2,0}R_{2,0}A_e\cos\theta \end{cases} \tag{3}$$

where $f_{l,0}$ is hydrostatic bearing force of bearing cavity, N; $q_{,0}$ is input flow, L/min; A_e is effective bearing area, m^2; θ is angle between bearing cavity and center line of axis, °.

Electromagnetic bearing force According to Maxwell force equation[16], the electromagnetic suspension forces of upper and lower magnetic poles are obtained as

$$f_{e,1,0} = f_{e,2,0} = 2k\cos\theta\frac{i_0^2}{h_0^2} \tag{4}$$

where $f_{e,0}$ is electromagnetic suspension force of magnetic pole, N; k is electromagnetic constant, H · m, $k = \mu_0 N^2 A_1/4$; i_0 is bias current of solenoid, A; μ_0 is air permeability, H/m, $\mu_0 = 4\pi \times 10^{-7}$; N is coil turns, dimensionless; A_1 is iron core area, m^2.

Flow balance equation Initially, the input flow of the bearing cavity is consistent with the output flow of the proportional valve.

$$\begin{cases} q_{1,0} = q_{f,1,0} \\ q_{2,0} = q_{f,2,0} \end{cases} \tag{5}$$

where $q_{1,0}$ is initial inflow of upper bearinng cavity, L/min; $q_{2,0}$ is initial inflow of underside bearing cavity, L/min.

Proportional equation of the suspension force The proportional relationship between electromagnetic suspension force and hydrostatic bearing force is set to realize coupling support between two bearing systems. The proportional coefficient is assumed to be K as

$$\frac{f_{e,0}}{f_{l,0}} = \left(\frac{ki_0^2}{h_0^2}\right) / \left(\frac{\mu q_0 A_e}{\bar{B}h_0^3}\right) = K \tag{6}$$

where K is magnetic-liquid coefficient, dimensionless.

Mechanics balance equation According to Newton's second law, and the mechanics balance equation of the rotor is obtained as

$$f_{e,1,0} + f_{l,2,0} - f_{e,2,0} - f_{l,,1,0} = 0 \tag{7}$$

1.2 Working state of single DOF support system

Under the external load, displacement of rotor is x, and upper and lower film thickness are h_1, h_2 respectively.

$$\begin{cases} h_1 = h_0 + x\cos\theta \\ h_2 = h_0 - x\cos\theta \end{cases} \tag{8}$$

Flow of proportional valve The displacement of the rotor is x, and the direction is downward. The control voltage of coil of proportional valve is u. The flows of the valve are as

$$\begin{cases} q_{f,1} = k_1(u_0 - u) \\ q_{f,2} = k_1(u_0 + u) \end{cases} \tag{9}$$

where q_f is output flow of proportional valve, L/min; u is control voltage, V.

Liquid resistance of bearing cavity When the film thicknesses of upper and lower bearing cavities are h_1 and h_2, the liquid resistances of the bearing cavities are as

$$\begin{cases} R_1 = \dfrac{\mu}{\bar{B}h_1^3} \\ R_2 = \dfrac{\mu}{\bar{B}h_2^3} \end{cases} \tag{10}$$

Hydrostatic bearing force According to Navier-Stokes equation, the hydrostatic bearing forces of upper and lower bearing cavities are obtained as

$$\begin{cases} f_{l,1} = 2p_1A_e\cos\theta = 2q_1R_1A_e\cos\theta \\ f_{l,2} = 2p_2A_e\cos\theta = 2q_2R_2A_e\cos\theta \end{cases} \tag{11}$$

where f_l is hydrostatic bearing force of bearing cavity, N; p is static pressure, Pa; q is input flow, L/min.

Electromagnetic suspension force According to Maxwell equation, the electromagnetic suspension forces of upper and lower magnetic poles are obtained as

$$\begin{cases} f_{e,1} = 2k\cos\theta\dfrac{(i_0 + i_c)^2}{(h_0 + x\cos\theta)^2} \\ f_{e,2} = 2k\cos\theta\dfrac{(i_0 - i_c)^2}{(h_0 - x\cos\theta)^2} \end{cases} \tag{12}$$

where f_e is electromagnetic suspension force, N; i_c is control current of solenoid, A.

Flow balance equation The influence of sensitive liquid path on bearing is ignored, and the flow balance equation between the bearing cavity and the proportional valve is obtained as

$$\begin{cases} q_1 = q_{f,1} - A_b\dot{h}_1 \\ q_2 = q_{f,2} - A_b\dot{h}_2 \end{cases} \tag{13}$$

where A_b is the equivalent extrusion area of bearing cavity, m^2.

Mechanics balance equation of rotor According to Newton's second law, the mechanics banlance equation of the rotor is obtained as

$$f_{e,1} + f_{l,2} - f_{e,2} - f_{l,1} = - m\ddot{x} \tag{14}$$

where m is rotor quality, kg.

1.3 Nonlinear autonomous equation of single DOF bearing system

Eq. (1) – Eq. (14) are comprehensively solved. Control voltage u of proportional valve and control current of solenoid i_c are assumed to be 0. The main parameters are shown in the Appendix 1. The dynamical equation of single DOF bearing system of MLDSB is obtained as

$$m\ddot{x} + f_k(\dot{x}, x) = 0 \tag{15}$$

1.4 Linearization of dynamic equation

Taylor series expansion of the dynamic equation of single DOF bearing is carried out with the initial state as the reference. The dynamic equation of linearization is obtained as

$$m\ddot{x} + c_l\dot{x} + k_l x = 0 \tag{16}$$

2 Equivalent linearization and parametric sensitivity analysis

2.1 Equivalent linearization of dynamic equations

According to Eq. (15), damping force and elastic force of single DOF autonomous bearing system of MLDSB have strong nonlinear features. Firstly, an equivalent linearization dynamical equation corresponding to nonlinear autonomous equation of single DOF bearing system is established as

$$m_e\ddot{x} + c_e\dot{x} + k_e x = 0 \tag{17}$$

where m_e is equivalent quality, kg; c_e is equivalent damping, N · s/m; k_e is equivalent stiffness, N/m.

Assume that the linear dynamical equation shown in Eq. (17) has stable periodic solution as follows.

$$x = a_t\cos\psi = a_t\cos(\omega_e t + \theta_1) \tag{18}$$

where a_t is equivalent amplitude, m; ω_e is equivalent natural frequency, Hz; θ_1 is equivalent vibration phase, rad; ψ is calculating parameter, dimensionless.

Eq. (18) is derived for time t, and the first and second derivatives are obtained as

$$\begin{cases} \dot{x} = -a_t\omega_e\sin\psi \\ \ddot{x} = -a_t\omega_e^2\cos\psi \end{cases} \tag{19}$$

Due to the low viscosity of seawater, the equivalent damping of single DOF autonomous bearing system of MLDSB is small. Therefore, amplitude a_t, equivalent damping ratio δ_e and equivalent natural frequency ω_e in Eq. (18) and Eq. (19) can be expressed as

$$\begin{cases} a_t = a_0 e^{-\delta_e t} \\ \delta_e = \dfrac{c_e}{2m_e} \\ \omega_e = \sqrt{\omega^2 - \delta_e^2} \\ \omega = \sqrt{\dfrac{k_e}{m_e}} \end{cases} \tag{20}$$

For convenience, the nonlinear bearing force $f_k(\dot{x}, x)$ in Eq. (15) is expressed in the form of Fourier series as

$$f_k(\dot{x}, x) = a_0 + \sum_{n=1}^{\infty}(a_n\cos n\psi + b_n\sin n\psi) \tag{21}$$

The first harmonic force load of the nonlinear vibration of single DOF bearing system of MLDSB is much larger than the second and the higher harmonic force load. Therefore, the second and higher harmonics can be ignored. The nonlinear element $f_k(\dot{x}, x)$ can be approximately expressed as

$$f_k(\dot{x}, x) = a_0 + a_1\cos\psi + b_1\sin\psi \tag{22}$$

Substituting Eq. (22) into Eq. (17).

$$m\ddot{x} + a_1\cos\psi + b_1\sin\psi = 0 \tag{23}$$

When the approximation of Eq. (18) and Eq. (19) is considered and constant force a_0 is removed, Eq. (23) is expressed as

$$m\ddot{x} - \frac{b_1}{\omega_e a_t}\dot{x} + \frac{a_1}{a_t}x = 0 \tag{24}$$

Equivalent mass m_e, equivalent damping c_e and equivalent stiffness k_e of single DOF autonomous bearing system are obtained by the equivalent linearization for Eq. (24).

$$\begin{cases} m_e = m \\ c_e = -\dfrac{1}{\pi\omega_e a_t}\displaystyle\int_0^{2\pi} f_k(a_t, \psi)\sin\psi \mathrm{d}\psi \\ k_e = \dfrac{1}{\pi a_t}\displaystyle\int_0^{2\pi} f_k(a_t, \psi)\cos\psi \mathrm{d}\psi \end{cases} \tag{25}$$

Since the variable x of function $f_k(a_t, \psi)$ is contained in the denominator and difficult to be solved, Taylor series expansion is performed on Eq. (16), and high order terms are reserved. Substituting it into initial condition ($\dot{x}_0 \neq 0$, $x_0 = 0$) as follows.

$$f_k(\dot{x}, x) = \Phi_1(x)c_l\dot{x} + \Phi_2(x)k_l x \tag{26}$$

Substituting Eq. (18), Eq. (19) and Eq. (26) into Eq. (25) as

$$\begin{cases} m_e = m \\ c_e = \Phi_3 c_l \\ k_e = \Phi_4 k_l \end{cases} \tag{27}$$

Since there is an unknown quantity a_t in Eq. (27), equivalent damping c_e and equivalent stiffness k_e are substituted into Eq. (20) as

$$a_t = a_0 e^{-\frac{c_e}{2m_e}t} \tag{28}$$

Equivalent damping c_e will be replaced with linear damping c_l as

$$a_t = a_0 e^{-\frac{c_l}{2m}t} \tag{29}$$

Substituting Eq. (29) into Eq. (27), and the expressions of equivalent mass m_e, equivalent damping c_e, and equivalent stiffness k_e can be obtained as

$$\begin{cases} m_e = m \\ c_e = c_l\left(1 + \dfrac{\Phi_{1,1}a_0^2}{4e^{\frac{c_l}{m}t}} + \dfrac{\Phi_{1,2}a_0^4}{8e^{\frac{2c_lt}{m}}} + \dfrac{5\,\Phi_{1,3}a_0^6}{64e^{\frac{3c_lt}{m}}}\right) \\ k_e = k_l\left(1 + \dfrac{3\,\Phi_{2,1}a_0^2}{4e^{\frac{c_l}{m}t}} + \dfrac{5\,\Phi_{2,2}a_0^4}{8e^{\frac{2c_lt}{m}}} + \dfrac{35\,\Phi_{2,3}a_0^6}{64e^{\frac{3c_lt}{m}}}\right) \end{cases} \tag{30}$$

By comparing Eq. (16) with Eq. (30), equivalent mass m_e is rotor mass m. And equivalent damping c_e/ equivalent stiffness k_e consist of 4 parts respectively. First part is linear damping c_l/ linear stiffness k_l, and the last three parts are high order minor terms which occurs during the process of Taylor series transform.

Substituting the parameters in Table 1 into Eq. (30), and the curves of linear damping, equivalent damping, linear stiffness and equivalent stiffness with time t are shown in Fig. 2.

According to Fig. 2, linear damping c_l/ linear stiffness k_l does not include time t and maintains constant. Equivalent damping c_e/ equivalent stiffness k_e of the first part is linear damping c_l/ linear stiffness k_l. And the high order minor terms in the last three parts are positive eternally.

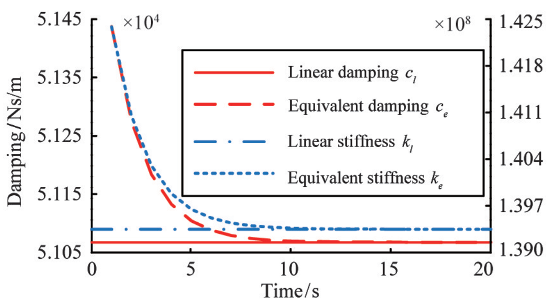

Fig. 2 The curve of damping and stiffness with time

2.2 Sensitivity analysis of relative error of stiffness and damping

Definition of relative error According to Eq. (16) and Eq. (30), linear damping c_l and linear stiffness k_l are only related to the design parameters. Equivalent damping c_e and equivalent stiffness k_e are not only influenced by design parameters, but also increases proportionally with time t.

Relative error δ_k is defined to indicate the difference between equivalent damping/stiffness and linear damping/stiffness as follows.

$$\begin{cases} \delta_c = \dfrac{c_e - c_l}{c_l} = \dfrac{1}{4}\Phi_{1,1}a_t^2 + \dfrac{1}{8}\Phi_{1,2}a_t^4 + \dfrac{5}{64}\Phi_{1,3}a_t^6 \\ \delta_k = \dfrac{k_e - k_l}{k_l} = \dfrac{3}{4}\Phi_{2,1}a_t^2 + \dfrac{5}{8}\Phi_{2,2}a_t^4 + \dfrac{35}{64}\Phi_{2,3}a_t^6 \end{cases} \tag{31}$$

Parameter sensitivity expression The relative error of stiffness δ_k is expressed in the following form.

$$g(\boldsymbol{\delta}, \boldsymbol{\alpha}, t) = 0 \tag{32}$$

The expression of function g in Eq. (32) is shown as

$$\begin{cases} \boldsymbol{g} = (g_c,\ g_k)^{\mathrm{T}} \\ \boldsymbol{g}_c = \delta_c - \dfrac{1}{4}\Phi_{1,1}a_t^2 - \dfrac{1}{8}\Phi_{1,2}a_t^4 - \dfrac{5}{64}\Phi_{1,3}a_t^6 \\ \boldsymbol{g}_k = \delta_k - \dfrac{3}{4}\Phi_{2,1}a_t^2 - \dfrac{5}{8}\Phi_{2,2}a_t^4 - \dfrac{35}{64}\Phi_{2,3}a_t^6 \end{cases} \tag{33}$$

When the initial value of parameter vector α_0 is constant, the initial value of state variable $\delta_{k,0}$ can be obtained as

$$g(\delta_{k,0}, \alpha_0, t) = 0 \tag{34}$$

In Eq. (34), the value $\Delta\delta_k$ can occur during the adjusting process of parameter vector $\boldsymbol{\alpha}$ as

$$g(\delta_{k,0} + \Delta\delta_k, \alpha_0 + \boldsymbol{\Delta\alpha}, t) = 0 \tag{35}$$

Eq. (35) can be expanded by binary Talyor series expansion as

$$\begin{aligned} & g(\delta_0 + \boldsymbol{\Delta\delta}, \alpha_0 + \boldsymbol{\Delta\alpha}, t) \\ & \quad = g(\delta_0, \alpha_0, t) + \boldsymbol{g_\delta \Delta\delta} + \boldsymbol{g_\alpha \Delta\alpha} \end{aligned} \tag{36}$$

Substituting Eq. (32) – Eq. (35) into Eq. (36).

$$\boldsymbol{\Delta\delta} = -\boldsymbol{g}_{\boldsymbol{\delta}}^{-1}\boldsymbol{g}_{\boldsymbol{\alpha}}\boldsymbol{\Delta\alpha} \tag{37}$$

In Eq. (38), $\boldsymbol{g_\delta}$ and $\boldsymbol{g_\alpha}$ represent second order Jacobian matrix ($\partial g/\partial\delta$) and 2 × 6 order Jacobian matrix ($\partial g/\partial\alpha$) respectively.

$$\begin{cases} \boldsymbol{g_\delta} = \begin{bmatrix} 1 & 0 \\ 0 & 1 \end{bmatrix} \\ \boldsymbol{g_\alpha} = \begin{bmatrix} g_{\alpha,1,1} & g_{\alpha,1,2} & g_{\alpha,1,3} & g_{\alpha,1,4} & g_{\alpha,1,5} & g_{\alpha,1,6} \\ g_{\alpha,2,1} & g_{\alpha,2,2} & g_{\alpha,2,3} & g_{\alpha,2,4} & g_{\alpha,2,5} & g_{\alpha,2,6} \end{bmatrix} \end{cases} \tag{38}$$

Eq. (37) can also be expressed in the following form.

$$\boldsymbol{\Delta\delta} = -\boldsymbol{S_\alpha \Delta\alpha} \tag{39}$$

where $\boldsymbol{S_\alpha} = \boldsymbol{g}_{\boldsymbol{\delta}}^{-1}\boldsymbol{g_\alpha}$ is 2 × 6 order sensitivity matrix. Since $\boldsymbol{g_\alpha}$ is identity matrix $\boldsymbol{I}$, the expression of $\boldsymbol{S_\alpha}$ is consistent with $\boldsymbol{g_\alpha}$ as

$$\boldsymbol{S}_{\alpha} = \boldsymbol{g}_{\alpha} = \begin{bmatrix} S_{\alpha,1,1} & S_{\alpha,1,2} & S_{\alpha,1,3} & S_{\alpha,1,4} & S_{\alpha,1,5} & S_{\alpha,1,6} \\ S_{\alpha,2,1} & S_{\alpha,2,2} & S_{\alpha,2,3} & S_{\alpha,2,4} & S_{\alpha,2,5} & S_{\alpha,2,6} \end{bmatrix} \quad (40)$$

Changing rule of relative error with time The relative errors of damping and stiffness are not only related to design parameters, but also demonstrate a trend of increasing first and decreasing with the time, as shown in Fig. 3 and Fig. 4.

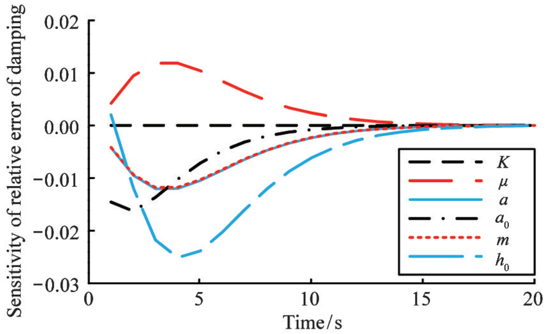

Fig. 3 Sensitivity of relative error of damping with time

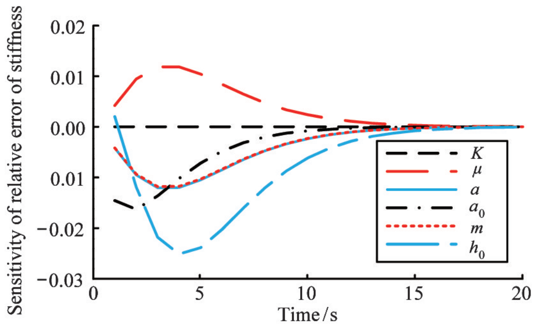

Fig. 4 Sensitivity of relative error of stiffness with time

3 Sensitivity analysis of bearing performances indicator

The influence of the relative error on the damping and stiffness of single DOF bearing system is mainly reflected in the change of the bearing performances of the autonomous bearing system of MLDSB.

Sensitivity of relative error of bearing indicator The bearing indicators of linear and equivalent linearization are denoted by subscript l and e. And the relative error $\boldsymbol{\Delta\xi}$ of two bearing indicators is obtained as

$$\boldsymbol{\Delta\xi} = \frac{\boldsymbol{\xi}_e - \boldsymbol{\xi}_l}{\boldsymbol{\xi}_l} \times 100\% \quad (41)$$

According to Eq. (39) − Eq. (43), the relative error $\boldsymbol{\Delta\xi}$ of the bearing indicator is implicit function of the parameters m, k_l, c_l, k_e, c_e.

$$\begin{cases} \Delta t_s = t_s(c_l, c_e) \\ \Delta J = J(m, k_l, c_l, k_e, c_e) \\ \Delta\gamma = \gamma(m, k_l, c_l, k_e, c_e) \\ \Delta f_n = f_n(k_l, k_e) \\ \Delta K_a = K_a(m, k_l, c_l, k_e, c_e) \end{cases} \quad (42)$$

According to Eq. (16) and Eq. (31), c_e and k_e are implicit functions of parameters c_l, k_l and Φ_{10} respectively. And c_l, k_l, Φ_{10} are implicit functions of parameters K, μ, a, a_0, m, h_0 respectively.

$$\begin{cases} c_e = c_e(c_l, \Phi_3, t) \\ k_e = k_e(c_l, \Phi_4, t) \\ c_l = c_l(\delta_1, h_0) \\ k_l = k_l(K, \delta_3, h_0) \\ \delta_1 = \delta_1(\mu, a) \\ \delta_3 = \delta_3(\mu, a) \\ \Phi_3 = \Phi_3(a_t, h_0) \\ \Phi_4 = \Phi_4(K, a_t, h_0) \\ a_t = a_t(a_0, m, c_l, t) \end{cases} \quad (43)$$

According to Eq. (33) − Eq. (38), the sensitivity between the relative error of the bearing indicator and the design parameters is established as

$$\boldsymbol{\Delta\xi} = \boldsymbol{\chi}_{\alpha}\boldsymbol{\Delta\alpha} \quad (44)$$

where $\boldsymbol{\chi}_{\alpha}$ is 5×6 order Jacobian matrix as

$$\boldsymbol{\chi}_{\alpha} = \begin{bmatrix} \chi_{\alpha,1,1} & \chi_{\alpha,1,2} & \chi_{\alpha,1,3} & \chi_{\alpha,1,4} & \chi_{\alpha,1,5} & \chi_{\alpha,1,6} \\ \chi_{\alpha,2,1} & \chi_{\alpha,2,2} & \chi_{\alpha,2,3} & \chi_{\alpha,2,4} & \chi_{\alpha,2,5} & \chi_{\alpha,2,6} \\ \chi_{\alpha,3,1} & \chi_{\alpha,3,2} & \chi_{\alpha,3,3} & \chi_{\alpha,3,4} & \chi_{\alpha,3,5} & \chi_{\alpha,3,6} \\ \chi_{\alpha,4,1} & \chi_{\alpha,4,2} & \chi_{\alpha,4,3} & \chi_{\alpha,4,4} & \chi_{\alpha,4,5} & \chi_{\alpha,4,6} \\ \chi_{\alpha,5,1} & \chi_{\alpha,5,2} & \chi_{\alpha,5,3} & \chi_{\alpha,5,4} & \chi_{\alpha,5,5} & \chi_{\alpha,5,6} \end{bmatrix} \quad (45)$$

Influence of design parameters on relative errors Substituting the parameters in Table 1 into Eq. (45), the histogram of the relative error of bearing indicator with design parameter is obtained as shown in Fig. 5.

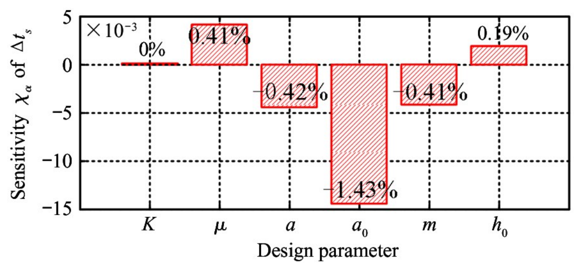

Fig. 5 Sensitivity of relative error of Δt_s ($t = 1$ s)

According to Fig. 5, the sensitivity of lubricant viscosity μ and film thickness h_0 to adjustment time is positive. It means that two parameters will lead to the increase of the adjustment time error. And the sensitivity of width of sealing side a, rotor mass m, and initial amplitude a_0 to adjustment time is negative. It means that 3 parameters will lead to the decrease of adjustment time error. The sensitivity of magnetic-liquid coefficient K to adjustment time is 0. It means that the error of adjustment time is not affected by the coefficient K.

According to Fig. 6, the sensitivity of width of sealing side a, initial amplitude a_0 and rotor mass m to dynamic stiffness is positive. It means that the error of dynamic stiffness will increase with the parameters. The sensitivity of magnetic-liquid coefficient K, lubricant viscosity μ and film thickness h_0 to dynamic stiffness is negative. It means that the error of dynamic stiffness will decrease with the parameters.

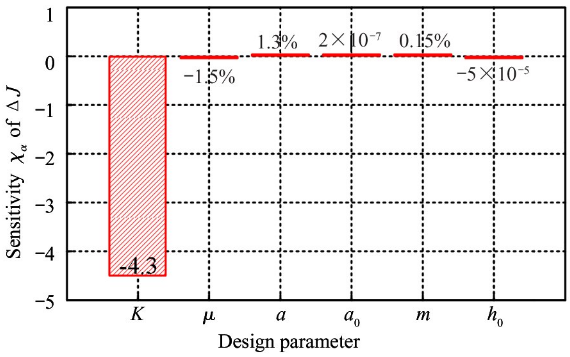

Fig. 6 Sensitivity of relative error ΔJ ($t = 1$ s)

According to Fig. 7, the sensitivity of magnetic-liquid proportionality coefficient K, lubricant viscosity μ and width of sealing side a to phase margin is positive. It means that the parameters will lead to the increase of phase margin error. The sensitivity of initial amplitude a_0, rotor mass m, and film thickness h_0 to phase margin is negative. It means that the parameters will lead to the decrease of phase margin error.

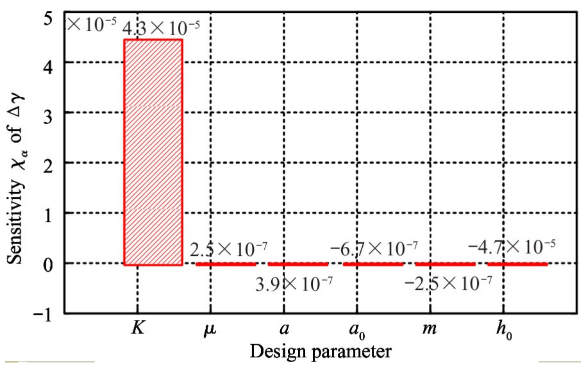

Fig. 7 Sensitivity of relative error $\Delta\gamma$ ($t = 1$ s)

4 Conclusions

(1) The sensitivity of relative error of damping and stiffness increases first and decreases with time, and the peak appears near 4 s.

(2) Initial amplitude is the major influence factor of natural frequency. Magnetic-liquid coefficient is the major influence factor of dynamic stiffness and phase margin. And film thickness is the major influence factor of amplitude coefficient.

(3) Film thickness and initial amplitude are the major influence factors of adjusting time, dynamic stiffness, phase margin, natural frequency and amplitude coefficient respectively.

(4) The sensitivity of relative error of adjustment time and natural frequency increases first and decreases with time, and then becomes stable.

References

[1] Sun B, Xu J, Xing C. Numerical and experimental investigations on the effect of mandrel feeding speed for high-speed rail bearing inner ring[J]. *The International Journal of Advanced Manufacturing Technology*, 2019, 100: 1993-2006

[2] Ruiz G, Anta J A, Tejero C F. The vapour-liquid transition of charge-stabilized colloidal suspensions: an effective one-component description [J]. *Journal of Physics Condensed Matter*, 2020, 249(15):3537-3547

[3] Zhao J H, Zhang B, Chen T, et al. Research on valve core's clamping stagnation of double flapper-nozzle servo valve[J]. *High Technology Letters*, 2019, 25(1): 65-73

[4] Torne S, Sheela A, Sarada N C. Investigation of the role of the alkalizing agent in sodium alginate liquid anti-reflux suspension[J]. *Current Drug Therapy*, 2020, 15(1): 53-60

[5] Jiang D, Zhao Y C, Wang D Y. Wavelet analysis of subway track monitoring with double magnetic suspension oscillator structure[J]. *Chinese Journal of Sensors and Actuators*, 2019,32(11):1682-1687 (In Chinese)

[6] Yang S Y, Li J H, Wu H T, et al. The nonlinear of the AMBs influenced by the controller's parameters[J]. *Chinese Journal of Scientific Instrument*, 2005, 26(8): 852-854 (In Chinese)

[7] Lv Y J, Liu H, Yu L. Stability and coupling dynamic behaviors of nonlinear journal active electromagnetic bearing-rotor system [J]. *Journal of Mechanical Strength*, 2005, 27(3): 301-306 (In Chinese)

[8] Zhang F, Jin Y Z, Wang X, et al. Exponential model of nonlinear liquid-film force of tilting-pad guide bearing and its application[J]. *Journal of Xi'an Jiaotong University*, 2017, 51(3): 72-79 (In Chinese)

[9] Lv Y J, Zhang Y F, Ji L F, et al. Analysis of dynamic characteristics of rotor nonlinear system supported by fixed-tilting pad journal bearings[J]. *Proceedings of the CSEE*, 2010, 30(20): 79-87 (In Chinese)

[10] He Y L. Calculation and simulation of the hybrid bearings nonlinear center trajectory[D]. Jinan: School of Mechanical Engineering, Shandong University, 2013 (In Chinese)

[11] Xu X J, Chen H D, Yan Y, et al. High-voltage DC inspection robot double coil magnetic suspension method [J]. *Computer Simulation*, 2019,36(8): 348-353, 357 (In Chinese)

[12] Li D S, Fan H L, Li Y. Fault diagnosis of rolling bear-

ings based on hilbert resonance demodulation method[J]. *Journal of Physics: Conference Series*, 2019, 1168(2): 1-6

[13] Zhao J H, Wang Q, Zhang B, et al. Influence of liquid film thickness on static property of magnetic-liquid double suspension bearing[C] // International Conference on Intelligent and Interactive Systems and Applications, Beijing, China, 2017: 809-816

[14] Huang W, Miao X, Hu G, et al. Experimental and shear bearing capacity studies of the assembled composite wall with bolted connections[J]. *The Structural Design of Tall and Special Buildings*, 2020, 29(6): 1-20

[15] Li Z, Yue F, Wang Q J. Analysis of vibration characteristics of spherical bearing of three-degree-of-freedom motor with liquid suspension[J]. *Journal of Low Frequency Noise Vibration and Active Control*, 2020: 40(1): 1-15

[16] Saini A, Kapaklis V, Wolff M. Electrical sensing in a magnetic liquid[J]. *IEEE Sensors Journal*, 2019, 19(16): 6948-6955

Appendix 1

Coefficients	Numerical value
$f_k(\dot{x}, x)$	$f_1(\dot{x}, x) + f_2(x) + f_3(x)$
$f_1(\dot{x}, x)$	$\left[\frac{\delta_1}{(h_0 + x\cos\theta)^3} + \frac{\delta_1}{(h_0 - x\cos\theta)^3}\right]\dot{x}$
$f_2(x)$	$\frac{\delta_2}{(h_0 + x\cos\theta)^2} - \frac{\delta_2}{(h_0 - x\cos\theta)^2}$
$f_3(x)$	$\frac{\delta_3}{(h_0 - x\cos\theta)^3} - \frac{\delta_3}{(h_0 + x\cos\theta)^3}$
δ_1	$\frac{2\mu A_e A_b \cos^2\theta}{B}$
δ_2	$2ki_0^2\cos\theta$
δ_3	$\frac{2\mu q_0 A_e \cos\theta}{B}$
c_l	$2\frac{\delta_1}{h_0^3}$
k_l	$(6 - 4K)\frac{\delta_3}{h_0^4}\cos\theta$
a_0	$\frac{1}{2\pi}\int_0^{2\pi} f_k(a, \psi)\,\mathrm{d}\psi$
a_1	$\frac{1}{\pi}\int_0^{2\pi} f_k(a, \psi)\cos\psi\,\mathrm{d}\psi$
b_1	$\frac{1}{\pi}\int_0^{2\pi} f_k(a, \psi)\,\Phi\sin\psi\,\mathrm{d}\psi$
$\Phi_1(x)$	$1 + \Phi_{1,1}x^2 + \Phi_{1,2}x^4 + \Phi_{1,3}x^6$
$\Phi_2(x)$	$1 + \Phi_{2,1}x^2 + \Phi_{2,2}x^4 + \Phi_{2,3}x^6$
$\Phi_{1,1}$	$\frac{6}{h_0^2}\cos^2\theta_1$
$\Phi_{1,2}$	$\frac{15}{h_0^4}\cos^4\theta_1$
$\Phi_{1,3}$	$\frac{28}{h_0^6}\cos^6\theta_1$
$\Phi_{2,1}$	$\frac{5 - 2K}{3 - 2K}\frac{2}{h_0^2}\cos^2\theta_1$
$\Phi_{2,2}$	$\frac{7 - 2K}{3 - 2K}\frac{3}{h_0^4}\cos^4\theta_1$
$\Phi_{2,3}$	$\frac{9 - 2K}{3 - 2K}\frac{4}{h_0^6}\cos^6\theta_1$
Φ_3	$1 + \frac{1}{4}\Phi_{1,1}a_t^2 + \frac{1}{8}\Phi_{1,2}a_t^4 + \frac{5}{64}\Phi_{1,3}a_t^6$
Φ_4	$1 + \frac{3}{4}\Phi_{2,1}a_t^2 + \frac{5}{8}\Phi_{2,2}a_t^4 + \frac{35}{64}\Phi_{2,3}a_t^6$

Continued Appendix 1

α	$(K, \mu, a, a_0, m, h_0)^{\mathrm{T}}$
δ	$(\delta_c, \delta_k)^{\mathrm{T}}$
$\Delta\alpha$	$(\Delta K, \Delta\mu, \Delta a_t, \Delta a_0, \Delta m, \Delta h_0)^{\mathrm{T}}$
$\Delta\delta$	$(\Delta\delta_c, \Delta\delta_k)^{\mathrm{T}}$
$g_{\alpha,1,1}$	0
$g_{\alpha,1,2}$	$\frac{\Phi_5 a_0 c_l t}{2\mu m} e^{-\frac{c_l}{2m}t}$
$g_{\alpha,1,3}$	$\frac{\Phi_5\ \Phi_6 a_0 c_l t}{2m} e^{-\frac{c_l}{2m}t}$
$g_{\alpha,1,4}$	$-\Phi_5 e^{-\frac{c_l}{2m}t}$
$g_{\alpha,1,5}$	$-\frac{\Phi_5 a_0 c_l t}{2m^2} e^{-\frac{c_l}{2m}t}$
$g_{\alpha,1,6}$	$\frac{3\ \Phi_7 a_t^2 \cos^2\theta}{h_0^3} - \frac{3\ \Phi_5 a_t c_l t}{2mh_0}$
$g_{\alpha,2,1}$	$-\frac{6\ \Phi_7 a_t^2 \cos^2\theta}{(3-2K)^2 h_0^2}$
$g_{\alpha,2,2}$	$\frac{\Phi_8 a_0 c_l t}{2\mu m} e^{-\frac{c_l}{2m}t}$
$g_{\alpha,2,3}$	$\frac{\Phi_6\ \Phi_8 a_0 c_l t}{2m} e^{-\frac{c_l}{2m}t}$
$g_{\alpha,2,4}$	$-\Phi_8 e^{-\frac{c_l}{2m}t}$
$g_{\alpha,2,5}$	$-\frac{\Phi_8 a_0 c_l t}{2m^2} e^{-\frac{c_l}{2m}t}$
$g_{\alpha,2,6}$	$\frac{3\ \Phi_9 a_t^2 \cos^2\theta}{(3-2K) h_0^3} - \frac{3\ \Phi_8 a_t c_l t}{2mh_0}$
Φ_5	$\frac{1}{2}\Phi_{1,1} a_t + \frac{1}{2}\Phi_{1,2} a_t^3 + \frac{15}{32}\Phi_{1,3} a_t^5$
Φ_6	$\Phi_{6,1} + \Phi_{6,2} + \Phi_{6,3}$
$\Phi_{6,1}$	$-\frac{2}{A_b}(B - 2b + A - 2a)$
$\Phi_{6,2}$	$-\frac{1}{A_e}(B - b + A - a)$
$\Phi_{6,3}$	$\frac{1}{B}\left(\frac{b + A - a}{6b^2} + \frac{a + B - b}{6a^2}\right)$
Φ_7	$1 + \frac{5a_t^2\cos^2\theta}{2h_0^2} + \frac{35a_t^4\cos^4\theta}{8h_0^4}$
Φ_8	$\frac{3}{2}\Phi_{2,1} a_t + \frac{5}{2}\Phi_{2,2} a_t^3 + \frac{105}{32}\Phi_{2,3} a_t^5$
Φ_9	$\Phi_{9,1} + \Phi_{9,2} + \Phi_{9,3}$
$\Phi_{9,1}$	$5 - 2K$
$\Phi_{9,2}$	$(7 - 2K)\frac{5\cos^2\theta a_t^2}{2h_0^2}$
$\Phi_{9,3}$	$(9 - 2K)\frac{35\cos^4\theta a_t^4}{8h_0^4}$
$\Delta\xi$	$(\Delta t_s\quad \Delta J\quad \Delta\gamma\quad \Delta f_n\quad \Delta K_a)^{\mathrm{T}}$
ξ_e	$(t_{s,e}\quad J_e\quad \gamma_e\quad f_{n,e}\quad K_{a,e})^{\mathrm{T}}$
ξ_l	$(t_{s,l}\quad J_l\quad \gamma_l\quad f_{n,l}\quad K_{a,l})^{\mathrm{T}}$

Continued Appendix 1

$\chi_{\alpha,1,1}$	$\left.\frac{\partial t_s}{\partial K}\right\|_0$	0
$\chi_{\alpha,1,2}$	$\left.\frac{\partial t_s}{\partial \mu}\right\|_0$	$\frac{\Phi_5}{2\Phi_3^2}\frac{a_t c_l}{\mu m}t$
$\chi_{\alpha,1,3}$	$\left.\frac{\partial t_s}{\partial a}\right\|_0$	$\frac{\Phi_5\Phi_6}{2\Phi_3^2}\frac{a_t c_l}{m}t$
$\chi_{\alpha,1,4}$	$\left.\frac{\partial t_s}{\partial a_0}\right\|_0$	$-\frac{\Phi_5}{\Phi_3^2}e^{-\frac{c_l}{2m}t}$
$\chi_{\alpha,1,5}$	$\left.\frac{\partial t_s}{\partial m}\right\|_0$	$-\frac{\Phi_5}{2\Phi_3^2}\frac{a_t c_l}{m^2}t$
$\chi_{\alpha,1,6}$	$\left.\frac{\partial t_s}{\partial h_0}\right\|_0$	$\frac{3}{\Phi_3^2}\frac{a_t}{h_0}\left(\Phi_7\frac{a_t}{h_0^2}\cos^2\theta-\frac{\Phi_5}{2}\frac{c_l}{m}t\right)$
$\chi_{\alpha,2,1}$	$\left.\frac{\partial J}{\partial K}\right\|_0$	$\frac{(\Phi_4k_l-m\omega^2)}{(\Phi_{10})^{\frac{1}{2}}(\Phi_{11})^{\frac{1}{2}}}\left[\frac{6\Phi_7}{(3-2K)^2}\frac{a_t^2k_l}{h_0^2}\cos^2\theta-4\Phi_4\frac{\delta_3}{h_0^4}\cos\theta\right]-4\frac{(\Phi_{10})^{\frac{1}{2}}}{(\Phi_{11})^{\frac{3}{2}}}(k_l-m\omega^2)\frac{\delta_3}{h_0^4}\cos\theta$
$\chi_{\alpha,2,2}$	$\left.\frac{\partial J}{\partial \mu}\right\|_0$	$\frac{1}{(\Phi_{10})^{\frac{1}{2}}(\Phi_{11})^{\frac{1}{2}}}\frac{k_l}{\mu}\left(\Phi_4k_l-m\omega^2\right)\left(\Phi_4-\frac{\Phi_8}{2}\frac{a_tc_l}{m}t\right)$ $+\frac{\Phi_3}{(\Phi_{10})^{\frac{1}{2}}(\Phi_{11})^{\frac{1}{2}}}\frac{c_l^2\omega^2}{\mu}\left(\Phi_3-\frac{\Phi_5}{2}\frac{a_tc_l}{m}t\right)-\frac{(\Phi_{10})^{\frac{1}{2}}}{(\Phi_{11})^{\frac{3}{2}}}\frac{1}{\mu}[(k_l-m\omega^2)k_l+c_l^2\omega^2]$
$\chi_{\alpha,2,3}$	$\left.\frac{\partial J}{\partial a}\right\|_0$	$\frac{(\Phi_4k_l-m\omega^2)}{(\Phi_{10})^{\frac{1}{2}}(\Phi_{11})^{\frac{1}{2}}}\left[(\Phi_{6.2}+\Phi_{6.3})\Phi_4k_l-\frac{\Phi_6\Phi_8}{2}\frac{a_tc_lk_l}{m}t\right]+\frac{\Phi_3\Phi_6}{(\Phi_{10})^{\frac{1}{2}}(\Phi_{11})^{\frac{1}{2}}}c_l^2\omega^2\left(\Phi_3-\frac{\Phi_5}{2}\frac{a_tc_l}{m}t\right)$ $-\frac{(\Phi_{10})^{\frac{1}{2}}}{(\Phi_{11})^{\frac{3}{2}}}[k_l(k_l-m\omega^2)(\Phi_{6.2}+\Phi_{6.3})+\Phi_6c_l^2\omega^2]$
$\chi_{\alpha,2,4}$	$\left.\frac{\partial J}{\partial a_0}\right\|_0$	$\frac{e^{-\frac{c_l}{2m}t}}{(\Phi_{10})^{\frac{1}{2}}(\Phi_{11})^{\frac{1}{2}}}[\Phi_8(\Phi_4k_l-m\omega^2)+\Phi_3\Phi_5c_l^2\omega^2]$
$\chi_{\alpha,2,5}$	$\left.\frac{\partial J}{\partial m}\right\|_0$	$\frac{(\Phi_4k_l-m\omega^2)}{(\Phi_{10})^{\frac{1}{2}}(\Phi_{11})^{\frac{1}{2}}}\left(\frac{\Phi_8}{2}\frac{a_tc_l}{m^2}t-\omega^2\right)+\frac{\Phi_3\Phi_5}{2(\Phi_{10})^{\frac{1}{2}}(\Phi_{11})^{\frac{1}{2}}}\frac{a_tc_l^3\omega^2}{m^2}t+\frac{(\Phi_{10})^{\frac{1}{2}}}{(\Phi_{11})^{\frac{3}{2}}}(k_l-m\omega^2)\omega^2$
$\chi_{\alpha,2,6}$	$\left.\frac{\partial J}{\partial h_0}\right\|_0$	$\frac{k_l}{h_0}\frac{(\Phi_4k_l-m\omega^2)}{(\Phi_{10})^{\frac{1}{2}}(\Phi_{11})^{\frac{1}{2}}}\left(\frac{3\Phi_8}{2}\frac{a_tc_l}{m}t-\frac{3\Phi_9}{3-2K}\frac{a_t^2}{h_0^2}\cos^2\theta-4\Phi_4\right)$ $+\frac{3\Phi_3}{(\Phi_{10})^{\frac{1}{2}}(\Phi_{11})^{\frac{1}{2}}}\frac{c_l^2\omega^2}{h_0}\left(\frac{\Phi_5}{2}\frac{a_tc_l}{m}t-\Phi_7\frac{a_t^2}{h_0^2}\cos^2\theta-\Phi_3\right)+\frac{(\Phi_{10})^{\frac{1}{2}}}{(\Phi_{11})^{\frac{3}{2}}}\left[\frac{4k_l}{h_0}(k_l-m\omega^2)+\frac{3c_l^2\omega^2}{h_0}\right]$
$\chi_{\alpha,3,1}$	$\left.\frac{\partial \gamma}{\partial K}\right\|_0$	$-\frac{2\Phi_3}{\Phi_{12}}c_l\omega\left[\frac{6\Phi_7}{(3-2K)^2}\frac{a_t^2k_l}{h_0^2}\cos^2\theta-4\Phi_4\frac{\delta_3}{h_0^4}\cos\theta\right]-\frac{4}{\Phi_{13}}\frac{\delta_3c_l\omega\cos\theta}{h_0^4}\left(180^\circ+\arctan\frac{-\Phi_3c_l\omega}{\Phi_4k_l-m\omega^2}\right)$
$\chi_{\alpha,3,2}$	$\left.\frac{\partial \gamma}{\partial \mu}\right\|_0$	$\frac{1}{\Phi_{12}}\frac{c_l\omega}{\mu}(\Phi_4k_l-m\omega^2)\left(\Phi_3-\frac{\Phi_5}{2}\frac{a_tc_l}{m}t\right)$ $-\frac{\Phi_3}{\Phi_{12}}\frac{k_lc_l\omega}{\mu}\left(\Phi_4-\frac{\Phi_8}{2}\frac{a_tc_l}{m}t\right)+\frac{1}{\Phi_{13}}\frac{mc_l\omega^3}{\mu}\left(180^\circ+\arctan\frac{-\Phi_3c_l\omega}{\Phi_4k_l-m\omega^2}\right)$
$\chi_{\alpha,3,3}$	$\left.\frac{\partial \gamma}{\partial a}\right\|_0$	$\frac{\Phi_6}{\Phi_{12}}c_l\omega(\Phi_4k_l-m\omega^2)\left(\Phi_3-\frac{\Phi_5}{2}\frac{a_tc_l}{m}t\right)-\frac{\Phi_3}{\Phi_{12}}c_l\omega\left[(\Phi_{6.2}+\Phi_{6.3})\Phi_4k_l-\frac{\Phi_6\Phi_8}{2m}k_la_tc_lt\right]$ $-\frac{1}{\Phi_{13}}c_l\omega[\Phi_6(k_l-m\omega^2)-k_l(\Phi_{6.2}+\Phi_{6.3})]\left(180^\circ+\arctan\frac{-\Phi_3c_l\omega}{\Phi_4k_l-m\omega^2}\right)$
$\chi_{\alpha,3,4}$	$\left.\frac{\partial \gamma}{\partial a_0}\right\|_0$	$\frac{1}{\Phi_{12}}c_l\omega e^{-\frac{c_l}{2m}t}[\Phi_5(\Phi_4k_l-m\omega^2)-\Phi_3\Phi_8k_l]$

Continued Appendix 1

$\chi_{\alpha,3,5}$	$\left.\frac{\partial\gamma}{\partial m}\right\vert_0$	$\frac{\Phi_5}{2\Phi_{12}}\frac{a_t c_l^2\omega}{m^2}t(\Phi_4 k_l - m\omega^2) - \frac{\Phi_3}{\Phi_{12}}c_l\omega\left(\frac{\Phi_8}{2}\frac{k_l a_t c_l}{m^2}t-\omega^2\right) - \frac{1}{\Phi_{13}}c_l\omega^3\left(180° + \arctan\frac{-\Phi_3 c_l\omega}{\Phi_4 k_l - m\omega^2}\right)$
$\chi_{\alpha,3,6}$	$\left.\frac{\partial\gamma}{\partial h_0}\right\vert_0$	$\frac{1}{\Phi_{12}}\frac{3c_l\omega}{h_0}(\Phi_4k_l-m\omega^2)\left(\Phi_5\frac{a_tc_l}{2m}t-\Phi_7\frac{a_t^2}{h_0^2}\cos^2\theta-\Phi_3\right) - \frac{\Phi_3}{\Phi_{12}}\frac{k_lc_l\omega}{h_0}\left(\frac{3\Phi_8}{2}\frac{a_tc_l}{m}t-\frac{3\Phi_9}{3-2K}\frac{a_t^2}{h_0^2}\cos^2\theta-4\Phi_4\right)-\frac{1}{\Phi_{13}}\frac{c_l\omega}{h_0}(k_l+3m\omega^2)\left(180°+\arctan\frac{-\Phi_3c_l\omega}{\Phi_4k_l-m\omega^2}\right)$
$\chi_{\alpha,4,1}$	$\left.\frac{\partial f_n}{\partial K}\right\vert_0$	$\frac{3\Phi_7}{(\Phi_4)^{\frac{1}{2}}}\frac{a_t^2\cos^2\theta}{(3-2K)^2h_0^2}$
$\chi_{\alpha,4,2}$	$\left.\frac{\partial f_n}{\partial \mu}\right\vert_0$	$-\frac{\Phi_8}{4(\Phi_4)^{\frac{1}{2}}}\frac{a_tc_l}{\mu m}t$
$\chi_{\alpha,4,3}$	$\left.\frac{\partial f_n}{\partial a}\right\vert_0$	$-\frac{\Phi_6\Phi_8}{4(\Phi_4)^{\frac{1}{2}}}\frac{a_tc_l}{m}t$
$\chi_{\alpha,4,4}$	$\left.\frac{\partial f_n}{\partial a_0}\right\vert_0$	$\frac{\Phi_8}{2(\Phi_4)^{\frac{1}{2}}}e^{-\frac{c_l}{2m}t}$
$\chi_{\alpha,4,5}$	$\left.\frac{\partial f_n}{\partial m}\right\vert_0$	$\frac{\Phi_8}{4(\Phi_4)^{\frac{1}{2}}}\frac{a_tc_l}{m^2}t$
$\chi_{\alpha,4,6}$	$\left.\frac{\partial f_n}{\partial h_0}\right\vert_0$	$\frac{3\Phi_8}{2}\frac{a_tc_l}{mh_0}t-\frac{3\Phi_9}{3-2K}\frac{a_t^2}{h_0^3}\cos^2\theta$
$\chi_{\alpha,5,1}$	$\left.\frac{\partial K_a}{\partial K}\right\vert_0$	$-\frac{4}{(\Phi_{10})^{\frac{1}{2}}(\Phi_{11})^{\frac{1}{2}}}\frac{k_l-m\omega^2}{h_0^4}\delta_3\cos\theta - \frac{2(\Phi_{11})^{\frac{1}{2}}}{(\Phi_{10})^{\frac{3}{2}}}\frac{(\Phi_4k_l-m\omega^2)\cos\theta}{h_0^2}\left[\frac{3\Phi_7}{(3-2K)^2}k_la_t^2\cos\theta-2\Phi_4\frac{\delta_3}{h_0^2}\right]$
$\chi_{\alpha,5,2}$	$\left.\frac{\partial K_a}{\partial \mu}\right\vert_0$	$\frac{1}{(\Phi_{10})^{\frac{1}{2}}(\Phi_{11})^{\frac{1}{2}}}\frac{k_l(k_l-m\omega^2)+c_l^2\omega^2}{\mu} - \frac{(\Phi_{11})^{\frac{1}{2}}}{(\Phi_{10})^{\frac{3}{2}}}\left[(\Phi_4k_l-m\omega^2)\left(\Phi_4\frac{k_l}{\mu}-\Phi_8\frac{k_la_tc_l}{2\mu m}t\right)+\Phi_3\frac{c_l^2\omega^2}{\mu}\left(\Phi_3-\Phi_5\frac{a_tc_l}{2m}t\right)\right]$
$\chi_{\alpha,5,3}$	$\left.\frac{\partial K_a}{\partial a}\right\vert_0$	$\frac{1}{(\Phi_{10})^{\frac{1}{2}}(\Phi_{11})^{\frac{1}{2}}}[(\Phi_{6.2}+\Phi_{6.3})(k_l-m\omega^2)k_l+\Phi_6c_l^2\omega^2] - \frac{(\Phi_{11})^{\frac{1}{2}}}{(\Phi_{10})^{\frac{3}{2}}}\left\{(\Phi_4k_l-m\omega^2)\left[(\Phi_{6.2}+\Phi_{6.3})\Phi_4k_l-\Phi_6\Phi_8\frac{a_tk_lc_l}{2m}t\right]+\Phi_3\Phi_6c_l^2\omega^2\left(\Phi_3-\Phi_5\frac{a_tc_l}{2m}t\right)\right\}$
$\chi_{\alpha,5,4}$	$\left.\frac{\partial K_a}{\partial a_0}\right\vert_0$	$\frac{-(\Phi_{11})^{\frac{1}{2}}}{(\Phi_{10})^{\frac{3}{2}}}(\Phi_4\Phi_8k_l+\Phi_3\Phi_5c_l^2\omega^2-\Phi_8m\omega^2)e^{-\frac{c_l}{2m}t}$
$\chi_{\alpha,5,5}$	$\left.\frac{\partial K_a}{\partial m}\right\vert_0$	$-\frac{1}{(\Phi_{10})^{\frac{1}{2}}(\Phi_{11})^{\frac{1}{2}}}(k_l-m\omega^2)\omega^2-\frac{(\Phi_{11})^{\frac{1}{2}}}{(\Phi_{10})^{\frac{3}{2}}}\left[(\Phi_4k_l-m\omega^2)\left(\frac{\Phi_8}{2}\frac{a_tc_l}{m^2}t-\omega^2\right)+\frac{\Phi_3\Phi_5}{2}\frac{a_tc_l^3\omega^2}{m^2}t\right]$
$\chi_{\alpha,5,6}$	$\left.\frac{\partial K_a}{\partial h_0}\right\vert_0$	$\frac{1}{(\Phi_{10})^{\frac{1}{2}}(\Phi_{11})^{\frac{1}{2}}}\left[\frac{4k_l}{h_0}(k_l-m\omega^2)+\frac{3c_l^2\omega^2}{h_0}\right] - \frac{(\Phi_{11})^{\frac{1}{2}}}{(\Phi_{10})^{\frac{3}{2}}}\left[\begin{array}{l}\frac{k_l}{h_0}(\Phi_4k_l-m\omega^2)\left(\frac{3\Phi_8}{2}\frac{a_tc_l}{m}t-\frac{3\Phi_9}{(3-2K)}\frac{a_t^2}{h_0^2}\cos^2\theta-4\Phi_4\right)\\ +3\Phi_3\frac{c_l^2\omega^2}{h_0}\left(\frac{\Phi_5}{2}\frac{a_tc_l}{m}t-\Phi_7\frac{a_t^2}{h_0^2}\cos^2\theta-\Phi_3\right)\end{array}\right]$

Zhao Jianhua, born in 1983. He received his Ph. D degree in 2013 from Yanshan University, China. He is currently an associate professor, postgraduate students' tutor of College of Mechanical Engineering of Yanshan University. He is mainly engaged in design calculation and performance analysis simulation of hydrostatic guide system of heavy CNC machine tools.